Optics Letters

Electrically pumped continuous-wave 1.3 μm quantum-dot lasers epitaxially grown on on-axis (001) GaP/Si

ALAN Y. LIU,[1,*] JON PETERS,[2] XUE HUANG,[3] DAEHWAN JUNG,[1] JUSTIN NORMAN,[1] MINJOO L. LEE,[4] ARTHUR C. GOSSARD,[1,2] AND JOHN E. BOWERS[1,2]

[1]Materials Department, University of California Santa Barbara, Santa Barbara, California 93106, USA
[2]Department of Electrical and Computer Engineering, University of California Santa Barbara, Santa Barbara, California 93106, USA
[3]Hewlett Packard Labs, Palo Alto, California 94304, USA
[4]Department of Electrical and Computer Engineering, University of Illinois, Urbana, Illinois 61801, USA
*Corresponding author: ayliu01@engineering.ucsb.edu

We demonstrate the first electrically pumped continuous-wave (CW) III–V semiconductor lasers epitaxially grown on on-axis (001) silicon substrates without offcut or germanium layers, using InAs/GaAs quantum dots as the active region and an intermediate GaP buffer between the silicon and device layers. Broad-area lasers with uncoated facets achieve room-temperature lasing with threshold current densities around 860 A/cm^2 and 110 mW of single-facet output power for the same device. Ridge lasers designed for low threshold operations show maximum lasing temperatures up to 90°C and thresholds down to 30 mA. © 2017 Optical Society of America

OCIS codes: (140.5960) Semiconductor lasers; (250.0250) Optoelectronics.

Efficient and low-cost on-chip light sources on silicon are necessary to meet the techno-economic requirements for high-volume silicon photonic applications, such as data communication [1]. III–V quantum-dot lasers epitaxially grown on silicon emitting around 1.3 μm have shown a promising performance, with the potential to be manufactured at scale at a low cost [1–3]. To fully capture their added value, these lasers should be compatible with existing silicon-based complementary metal-oxide-semiconductor (CMOS) foundry process flows to enable their integration with other photonic devices on a common silicon substrate. We and other groups have previously demonstrated high-performance continuous-wave 1.3 μm quantum-dot lasers epitaxially grown on silicon [2–4]. However, these past works utilized intentionally offcut silicon substrates to suppress antiphase disorder arising from the III–V (polar) on silicon (non-polar) heteroepitaxy, and as such, they are not compatible with standard silicon-based CMOS processing, which requires nominal (001) silicon.

Previous work on III–V lasers epitaxially grown on on-axis (001) silicon include continuous-wave optically pumped 1.3 μm InAs quantum-dot microdisk lasers on patterned (001) silicon [5] and the pulsed operation of optically pumped 1.3 μm InGaAs/InP distributed-feedback lasers on patterned (001) silicon [6]. Continuous-wave operation under electrical pumping is required for practical device applications but is more challenging compared to optical pumping due to the more complicated device fabrication and carrier transport issues that may not be present under optical pumping. So far, the only report of an electrically pumped laser on on-axis (001) silicon is the pulsed operation of an InGaAs/GaAs quantum-well laser on GaP/Si emitting at 1 μm [7]. Continuous-wave operation under electrical pumping has thus far not been demonstrated. In this work, we report the first demonstration of an electrically pumped continuous-wave III–V quantum-dot laser operating at room temperature and above that has been epitaxially grown on on-axis GaP/silicon substrates without offcut or germanium buffers.

The epitaxial laser stack was grown on a GaP/Si (001) template provided by NAsP III–V GmbH. The original template was a 775 μm thick (001) on-axis p-doped Si substrate with a 200 nm thick n-doped Si homo-epitaxial buffer and a subsequent 45 nm thick n-doped GaP nucleation layer deposited by metal organic chemical vapor phase epitaxy [8]. A 2.3 μm GaAs buffer layer was then grown on the GaP/Si template in a solid-source molecular beam epitaxy (MBE), as previously reported in [7]. A thermal annealing cycle was employed after the growth of the GaAs buffer to facilitate dislocation annihilation [7]. Following this, an InAs quantum-dot laser embedded in a GaAs/AlGaAs graded-index separate confinement heterostructure (waveguide was re-grown on top of the GaAs buffer). The active region consisted of seven stacks of InAs quantum-dot layers embedded in 8 nm In$_{0.15}$Ga$_{0.85}$As quantum wells, which were separated by partially p-modulation-doped GaAs barriers, following previously reported conditions [9]. The same laser structure was also grown on a GaAs substrate for comparison.

The as-grown material was then processed into deeply etched ridge waveguide lasers with varying stripe widths using standard dry etching and metallization techniques. The Ti/Pt/Au p-contact was deposited on top of the etched mesa, and an AuGe/Ni/Au n-contact metal was deposited on the exposed nGaAs layers. Two types of laser geometries were fabricated: the first are broad-area lasers with 20 μm wide stripe widths to ascertain the material quality, and the second are narrow-ridge waveguide lasers with smaller stripe widths between 2–10 μm wide and cavity lengths between 750–1500 μm long. Laser facets were formed by either cleaving or polishing. High-reflection facet coatings were applied to the narrow-ridge waveguide devices, with ~95% reflectors on the back facet and either ~55% [single distributed Bragg reflector (DBR) pair] or ~80% (double DBR pair) on the front. Optical and scanning electron microscope images of the fabricated devices are shown in Fig. 1. All laser measurements presented in this Letter were conducted in continuous-wave mode.

Prior to laser growth, the GaAs/GaP/Si buffer was characterized with electron channeling contrast imaging, which revealed a threading dislocation density of $\sim 3 \times 10^8/cm^2$. Figure 2 shows a room-temperature photoluminescence (PL) comparison of the as-grown laser material on GaP/Si to the reference structure grown on GaAs under 1.17 W/cm² of excitation from a 785 nm pump laser. Both samples show a similar peak wavelength of 1280 nm, while the laser on GaP/Si has a relative peak intensity of 57% compared to the reference sample on GaAs. The full width at half-maximum values of the PL
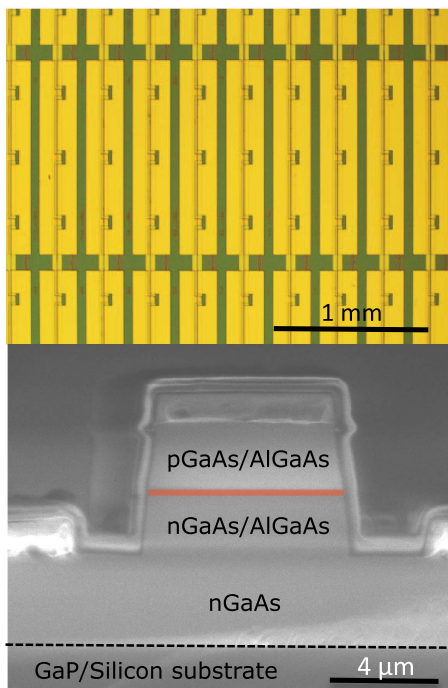

Fig. 2. Room-temperature PL comparison of the as-grown laser stacks on GaP/Si to a reference laser grown on GaAs substrate under an incident pump-power density of 1.17 W/cm². The full width at half-maximum values are 41 and 54 meV for the samples on GaAs and GaP/Si, respectively.

peaks are 41 and 54 meV for the sample on GaAs and GaP/Si, respectively. Figure 3 shows the continuous-wave light-current (LI) comparisons of five broad-area lasers on GaAs to five on GaP/Si, with the exact same cavity size (2 mm × 20 μm) and no extra high-reflection coatings applied to the facets. The lowest threshold current (densities) of the aforementioned devices are 190 mA (475 A/cm²) for lasers on GaAs and 345 mA (862 A/cm²) for GaP/Si. The corresponding differential quantum efficiencies of the aforementioned devices are 16.87% for the laser on GaAs and 8.80% for the one on GaP/Si. As shown in the same figure, single-facet output powers up to 110 mW were obtained from the lasers on GaP/Si. It is interesting to note that the relative percentage increase in the threshold current density and the decrease in the differential efficiency are

Fig. 1. Top: an optical micrograph of rows of fabricated narrow-ridge waveguide lasers prior to cleaving or dicing. The continuous vertical stripes are the III–V laser mesas, while the gold pads on the left and right of the mesa are the n and p probe pads, respectively. Bottom: a scanning electron microscope image of the cleaved cross section for a narrow-ridge waveguide laser on GaP/silicon. The shaded red area indicates the approximate position of the active region.
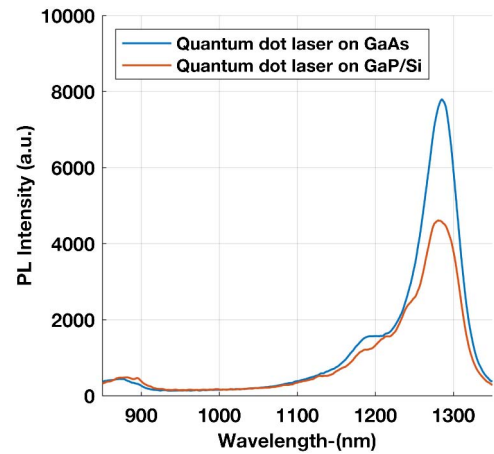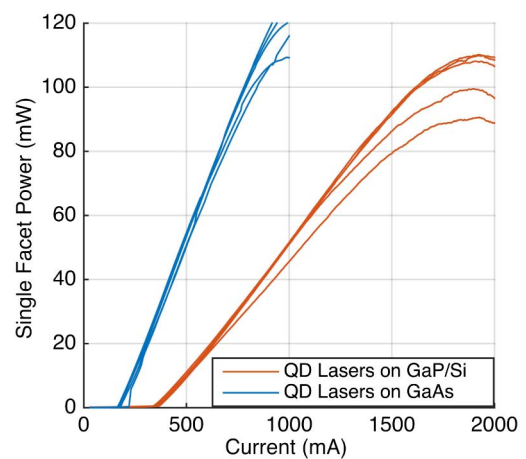

Fig. 3. Room-temperature light-versus-current comparisons of 2 mm long by 20 μm wide broad-area lasers without facet coatings on GaAs (blue) and GaP/Si (red). Five devices of each type are shown. The lowest threshold current (densities) of the aforementioned devices is 190 mA (475 A/cm²) for lasers on GaAs and 345 mA (862 A/cm²) for GaP/Si, with corresponding differential quantum efficiencies of 16.87% and 8.80%.
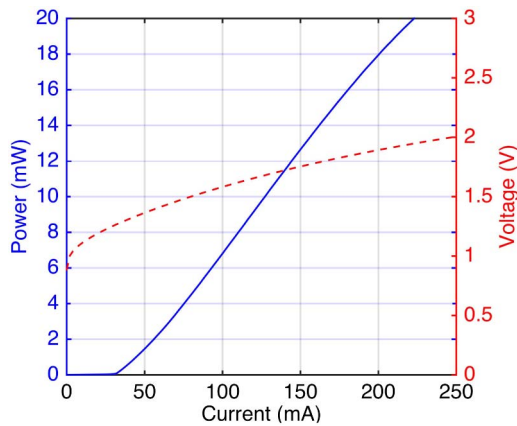
Fig. 4. Room-temperature continuous-wave light-current-voltage curve for an HR/HR coated (95%/55%) 750 µm × 4 µm laser with a threshold of 32 mA.

roughly the same, suggesting a decrease in injection efficiency η_i, an increase in optical loss α_i, or a combination of both for the devices on GaP/Si.

Narrow-ridge waveguide lasers were fabricated via facet polishing followed by high-reflection coating of the facets. Figure 4 shows room-temperature light-current-voltage measurements of a 750 µm × 4 µm device with a 32 mA threshold and a slope efficiency of 0.106 W/A. A plot of the threshold current versus the ridge width for 68 different measured lasers with cavity lengths ranging from 750 to 1500 µm is shown in Fig. 5. The threshold decreases as expected for smaller cavities, with the lowest threshold being 30 mA. We hypothesize that the statistical scatter is mostly due to the chipping of the facet material from the high-aspect ratio waveguides during the polishing process, as confirmed by a visual inspection. Figure 6 shows a typical room-temperature lasing spectrum for a laser on GaP/Si. The lasing wavelength of 1280 nm matches closely with the measured photoluminescence peak.

Figure 7 demonstrates high-temperature continuous-wave operation of a longer device (1500 µm × 3.5 µm) up to 90°C. There is a discontinuously large increase in the threshold

Fig. 6. (a) Coarse electroluminescence spectra of a 1500 µm × 3.5 µm HR-coated (95%/55%) laser below (70 mA) and above threshold (80 mA) at room temperature showing ground-state lasing at 1280 nm. (b) High-resolution scan of the above threshold lasing spectrum for the same device at 270 mA showing the many Fabry–Perot longitudinal modes centered around 1280 nm.

between 80°C–90°C, which we think is due to the saturated ground-state gain being unable to compensate for the cavity loss, resulting in lasing from the excited state. A plot of the CW threshold current versus the stage temperature for the devices in Fig. 7, along with several other measured lasers, is shown in Fig. 8. The average characteristic temperature T_0, as extracted by fitting the increase in threshold as an exponential function
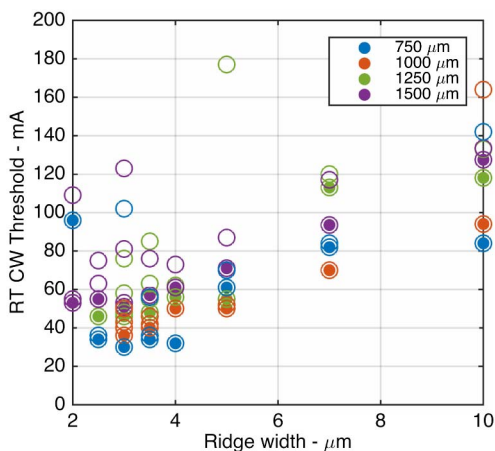

Fig. 5. Room-temperature continuous-wave threshold currents for 68 different HR/HR coated (95%/55%) ridge waveguide lasers of various cavity sizes.
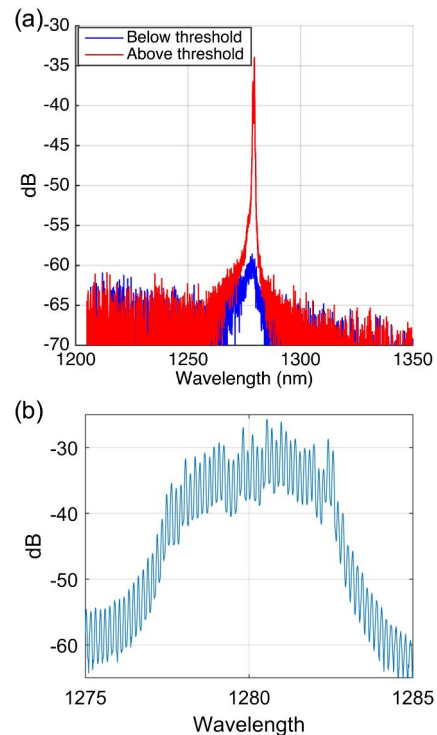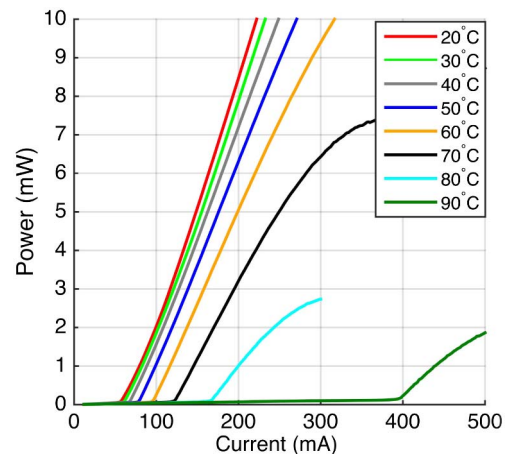

Fig. 7. 1500 µm × 3.5 µm device showing continuous-wave lasing up to 90°C. At 20°C, the output power was 26.6 mW at a bias current of 500 mA.
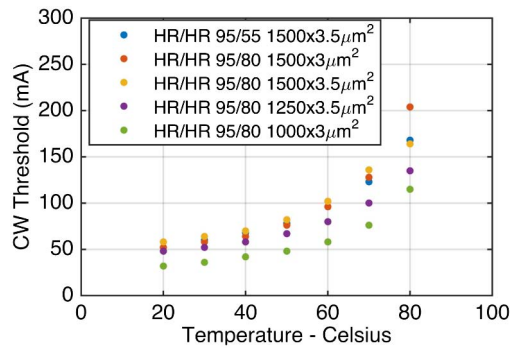
Fig. 8. Plot of the threshold current versus the stage temperature for five different laser devices. The average characteristic temperature T_0 is ~100 K between 20°C–40°C and ~40 K between 40°C–80°C.

of temperature, $I_{\text{th}}(T) = I_0 \times \exp(\frac{T}{T_0})$, is ~100 K between 20°C–40°C and ~40 K between 40°C–80°C. This behavior is roughly in line with what we have previously observed for similar lasers grown on Ge/Si substrates [4,9].

We note that the sidewalls for the deeply etched mesa stripes defining the laser cavity showed significant roughness from the fabrication process. While not a serious issue for broad-area devices with wide stripe widths, the roughness likely limited the performance of the narrow-ridge waveguide lasers where the mode sees a higher overlap with the sidewalls, resulting in increased sidewall scattering loss (and sidewall recombination current). We therefore expect further improvements in device performance from optimized processing.

We have presented the first electrically pumped continuous-wave III–V quantum-dot lasers epitaxially grown on on-axis (001) silicon without offcut or germanium layers. Narrow-ridge waveguide lasers show thresholds down to 30 mA and lasing to 90°C, while broad-area lasers with threshold current densities of 862 A/cm^2 and output powers up to 110 mW have been demonstrated. This work demonstrates the compatibility of high-performance monolithic III–V light sources with on-axis silicon substrates and their potential for foundry integration.

REFERENCES

1. Z. Zhou, B. Yin, and J. Michel, Light Sci. Appl. **4**, e358 (2015).
2. A. Y. Liu, S. Srinivasan, J. Norman, A. C. Gossard, and J. E. Bowers, Photon. Res. **3**, B1 (2015).
3. S. Chen, W. Li, J. Wu, Q. Jiang, M. Tang, S. Shutts, S. N. Elliott, A. Sobiesierski, A. J. Seeds, I. Ross, P. M. Smowton, and H. Liu, Nat. Photonics **10**, 307 (2016).
4. A. Y. Liu, C. Zhang, J. Norman, A. Snyder, D. Lubyshev, J. M. Fastenau, A. W. Liu, A. C. Gossard, and J. E. Bowers, Appl. Phys. Lett. **104**, 041104 (2014).
5. Y. Wan, Q. Li, A. Y. Liu, A. C. Gossard, J. E. Bowers, E. L. Hu, and K. M. Lau, Opt. Lett. **41**, 1664 (2016).
6. Z. Wang, B. Tian, M. Pantouvaki, J. V. Campenhout, C. Merckling, and D. V. Thourhout, in *Conference on Lasers and Electro-Optics* (Optical Society of America, 2016), paper SW4M.3.
7. X. Huang, Y. Song, T. Masuda, D. Jung, and M. Lee, Electron. Lett. **50**, 1226 (2014).
8. K. Volz, A. Beyer, W. Witte, J. Ohlmann, I. Németh, B. Kunert, and W. Stolz, J. Cryst. Growth **315**, 37 (2011).
9. A. Y. Liu, C. Zhang, A. Snyder, D. Lubyshev, J. M. Fastenau, A. W. Liu, A. C. Gossard, and J. E. Bowers, J. Vacuum Sci. Technol. B **32**, 02C108 (2014).